Form function relationships in dragonfly mandibles under an evolutionary perspective

Alexander Blanke[1*], Helmut Schmitz[2], Alessandra Patera[3,4], Hugo Dutel[1], Michael J. Fagan[1]

[1] Medical and Biological Engineering Research Group, School of Engineering, University of Hull, Hull HU6 7RX, UK

[2] Institute for Zoology, University of Bonn, Poppelsdorfer Schloss, 53115 Bonn, Germany

[3] Swiss Light Source, Paul Scherrer Institut, Villigen, 5232, Switzerland

[4] Centre d'Imagerie BioMedicale, Ecole Polytechnique Federale de Lausanne, 1015 Lausanne, Switzerland

* corresponding author

Corresponding author contact information:

Alexander Blanke

Medical and Biological Engineering Research Group, School of Engineering, University of Hull, Hull HU6 7RX, UK; e-mail address: a.blanke@hull.ac.uk

Abstract

Functional requirements may constrain phenotypic diversification but may also foster it. For insect mouthparts, the quantification of the relationship between shape and function in an evolutionary framework remained largely unexplored. Here, the question of a functional influence on phenotypic diversification for dragonfly mandibles is assessed with a large scale biomechanical analysis covering nearly all anisopteran families using finite element analysis in combination with geometric morphometrics. A constraining effect of phylogeny could be found for shape, the mandibular mechanical advantage and certain mechanical joint parameters while stresses and strains, the majority of joint parameters and size are not influenced by shared ancestry. Furthermore, joint mechanics are not correlated with strain nor with the mandibular mechanical advantage and size effects virtually play no role for shape or mechanical variation. The presence of mandibular strengthening ridges shows no phylogenetic signal except for one ridge peculiar to Libelluloidea and ridge presence is also not correlated with each other. The results suggest that functional traits are more variable at this taxonomic level and that they are not influenced by shared ancestry. At the same time results contradict the widespread idea that mandibular morphology mainly reflects functional demands at least at this taxonomic level. The varying functional factors rather lead to the same mandibular performance as expressed by the mechanical advantage which suggests a many-to-one mapping of the investigated parameters onto the same narrow mandibular performance space.

Keywords

insect, dragonfly, finite element analysis, geometric morphometrics, material properties, mandible, geometry, phylogeny

Introduction

Insects show a remarkable mouthpart disparity, but the factors leading to this disparity are poorly understood. It is unclear at which levels mouthpart form is mainly regulated by functional requirements such as food spectrum or weight optimization, and when phylogeny or development play the major role [1–4]. Surprisingly few studies have assessed the mechanical performance of insect mandibles. So far, insect mandible bite performance has been shown to be influenced by the origin and attachment sites of the mandible muscles [5–8], muscle mass, muscle physiology and structure, as well as innervations [8–12]. Distantly related lineages such as beetles and grasshoppers show larger differences in mandible shape [13,14] which is presumably related to different food types [15–17].

Due to the high diversity of mouthpart shape across insects, influences of function and phylogeny are difficult to separate from each other, and from other factors such as the ecological niche or development. In this context, dragonflies represent a useful model system, since their life style and mouthpart morphology is comparably uniform. All dragonflies are aerial hunters preying on other winged insects such as flies, mosquitoes or even other dragonflies which they often consume on the wing, and they show the same larval development with several stages of aquatic larvae before molting (with a drastic morphological reorganisation) to the adult [18]. Mandible gross morphology is also the same among all adult dragonflies with a row of sharp teeth-like structures (incisivi) in apical position and another row of subapical incisivi in the mesal area and a similar shape overall [19,20]. Thus, their ecomorphology with regards to food uptake and potential developmental constraints is largely similar. Given these similarities, it should be possible to study the influence of small morphological variations on function with the background of a phylogenetic framework. Here, we use a group of dragonfly species which show the same muscular arrangement, the same joint type and the same gross mandibular form, to investigate the interplay of shape and biomechanics and the influence of phylogeny on these factors. In

particular, we study whether shape, biomechanics or size show phylogenetic signal and whether shape, biomechanics and size correlate with each other.

Materials and methods

We used the damselfly *Calopteryx virgo* as the outgroup and a range of dragonfly species (Odonata: Anisoptera) covering all currently recognized families except Chlorogomphidae and Synthemistidae (Table 1) for our analyses. The resulting dataset consisted of 21 mandible models. All samples are housed in the alcohol collection of the Zoological Research Museum Alexander Koenig (ZFMK). For the sake of brevity species will be named only with their genus name in the following. The description of morphological structures follows the terminology of Beutel et al. [21]. New terms for mandible structures not covered so far by the literature are defined at the appropriate points in the text when they are first used.

Bite force measurements

In order to understand how bite force influences strain levels, we measured the bite force of five out of the 21 studied species (*Sympetrum, Cordulegaster, Onychogomphus, Aeshna* and *Anax*) covering a wide body size range and taxonomic range which were available locally (collection permit 67.1-2.03.20-33/13-M (ZFMK)). Bite force measurements were performed using a bespoke setup described in other studies [22,23]. Briefly, it consisted of a custom built specimen fixation device and an adjustable piezoelectric mini force sensor (SKB pinforce sensor Z18152X2A3sp and Z18152X2A7sp, Kistler, Winterthur, Switzerland). Bite series were subsequently filtered (Butterworth, low pass, 4th order, 50 Hz cut-off, recursive). Single bites were identified, when the force time curve showed a continuous increase of at least 0.02 N, an unambiguously identifiable absolute maximum, absence of local minima between biting onset and peak force, and absence of movement artefacts due to movement of the insect. Please refer to David et al. [22,23] for further details.

Mechanical testing via nano-indentation

We used the same set of freshly collected dragonflies for measuring the material parameters of the mandibles. Mandibles were excised and embedded in Epoxy Resin L (R&G Faserverbundwerkstoffe, Germany). Semi-thin cross-sections were cut from the embedded samples using a microtome equipped with a 6 mm diamond knife (company Diatome, Switzerland) in 4µm slices until a suitable cross-sectional profile was identified, at which point the surface was polished by cutting a few ultrathin sections at 0.5 µm.

An area function covering all contact depths obtained in the measurements was established by indenting a polymethyl methacrylate test specimen of known hardness and modulus. To obtain data from cuticle that is fully saturated with water, a drop of distilled water was put on the faces of the resin blocks for at least 20min before the test which was sufficient to saturate the material and stabilize the material properties [24]. After this, an appropriate position for indentation was located and another drop of distilled water placed between the surface and tip to ensure wet cuticle properties. After another 5-10min the water was removed again and measurements (N=6-15 per sample at locations at least 4µm apart) were taken in rapid succession, typically every 15s. This measurement process followed a protocol optimized in earlier studies [24,25] and ensured that wet cuticle properties were measured. Contact depths ranged from 130-1500nm, with a maximum load during indentation of 1500µN and loading and unloading rates of 20µN/s, and a 2 s holding time at peak load to compensate for material creep. Hardness (H) and reduced Young's modulus (E) were both determined from the unloading portions of the load–displacement curves following established procedures [26].

3D model generation

To obtain models of the mandibles suitable for finite element analysis (FEA), we performed synchrotron radiation micro computed-tomography (SR-µCT). For preparation, collected odonates were either freshly placed into Bouin solution [27] or taken from the alcohol

collection of the Zoological Research Musem A. Koenig (ZFMK). Samples were washed in 70% EthOH, critical point dried (Model E4850, BioRad), and mounted on specimen holders. SR-µCT was carried out at the Deutsches Elektronen Synchrotron (beamlines DORIS III/BW2 and PETRA III/IBL P05, DESY, Hamburg, Germany) or at the Swiss Light Source of the Paul-Scherrer Institut (PSI, Villigen, Switzerland, beamline TOMCAT) using established procedures [28–30]. Subsequent segmentation of the reconstructed image stacks was accomplished with ITK-SNAP [31]. STL files were then imported into AVIZO (v. 9.0.1; FEI; USA) for generation of the tetrahedral meshes which were then exported in UNV-format for import into the finite element solver. We also plotted the cuticle thickness on the 3D models of the mandibles in order to correlate mandible thickness with strain patterns from the finite element analysis.

Finite Element Analysis (FEA)

We used the finite element solver ANSYS (v. 14.5; ANSYS, Inc., USA) for the FEA. The models typically consisted of ~175,000 second-order tetrahedral elements (ANSYS type SOLID92). The models were minimally constrained at one node in x, y and z direction at the anterior and posterior joints thus allowing free rotation about the joint axis. Nodes over the area of the muscle attachment site were connected individually by LINK180 elements to an additional node in space so that the direction of the muscle was defined correctly. The measured material properties were not significantly different between the five species measured and between dry (6.7±1.2 - 8.9±0.9 GPa) and rewetted (5.4±0.9 - 9.8±1.7 GPa) mandibles. Thus, we used the mean Young's modulus over all measurements for rewetted mandibles (8.8GPa). We applied a unit load of 1N to the mandible tips to allow for comparison of strain patterns and thus mouthpart performance in these differently sized mandibles. Bite force measurements for a subset of the species investigated show that mandible bite forces range between 0.3 - 1.8N depending on the species investigated [22,23].

After the FE solutions were complete, first and third principal strain distributions were displayed on the 3D models, which correspond to the most tensile (ε1) and most compressive (ε3) strains at each point of the model. Strain values were also extracted from the middle part of each mandible (the mesal area in posterior view) in order to compare these between species without taking into account local peak strains at the muscle insertions, bite points and joints.

Joint mechanics

To study a potential correlation of mandible joint performance with phylogeny, we used the ANSYS output for the joint reaction forces (JRF). The two mandible joints and the apical mandible define a triangle (henceforth called the joint-tip triangle; landmarks 1, 10 and 13 in Figure 1) where the small side of this triangle defines a virtual axis between the anterior and posterior joint which was used to align the mandibles to each other. The JRF vectors were then imported into Blender and plotted onto these joint-tip triangles to provide a visual representation of the variance in the size and direction of the mandibles' JRFs. Joint-tip triangles were scaled to a length of one with respect to the joint axis and aligned along this axis to allow for comparison of the magnitude and direction of the JRFs in 3D (Supplemental 3D model S2). Additionally we calculated the mechanical advantage (MA) for each mandible. As in vertebrates [32,33] the dicondylous insect mandible can be modeled as a third order lever. The mandible closing MA is the ratio between the inner lever arm, which is the distance between the point of application of the input force (here the adductors insertion) and the mandible joint, and the outer lever arm, which is the distance between the mandible joint and the biting point at the tip of the mandible. The MA thus gives a proportion of the muscle force that is transferred to the food item during biting. In a comparative context, the MA can be a useful proxy to assess the biomechanical disparity among taxa, which might be decoupled from the morphological disparity [34,35]. We used the kappa statistic as implemented in the 'geomorph' package [36,37] to test for potential phylogenetic signal in JRFs and MA and we

calculated phylogenetically independent contrasts (PICs) to test for correlations between JRFs, size, mechanical advantage (MA) and the biomechanical data represented by the median of the 1000 nodes showing the highest displacements in the median region of each mandible (median of the peak displacements, henceforth "MPDs"). The phylogeny used, including branch lengths, was obtained from Letsch et al. [38] and pruned in R using the phytools package [39] to represent the biomechanical taxon sampling.

Geometric morphometrics

A series of 18 3D landmarks, 13 homologous and five semilandmarks was chosen to represent the 3D shape of each mandible (Figure 1). All landmarks were exported from Blender (v. 2.77, www.blender.org) from STL models of the mandibles for geometric morphometric analysis with the "shapes", "geomorph", "morpho", "caper", "phytools" and "ape" packages provided within the statistics software R [39–42]. After a Procrustes superimposition [43,44] to correct for effects of rotation, translation and size, a principal component analysis (PCA) was performed to investigate the variance associated with the shape variables expressed as principal component scores. Phylogenetic ANOVA as implemented in geomorph ('procD.pgls') was used to investigate the association of shape (all principal components) with size, MPDs, JRFs and the MA. A multivariate K-statistic [36,37] incorporated within the 'geomorph' package in R was used to account for potential phylogenetic signal in the shape data and in the biomechanical data represented by the MPDs of each mandible. See Adams [36] and Blomberg et al. [37] for an estimate of statistical power in relation to sample size. In addition, we tested a potential pairwise correlation of mandible ridges using Pagel's pairwise correlation test of discrete datasets [45] as implemented in the 'phytools' package for R [39] again taking the phylogeny published in Letsch et al. [38] as a basis. To test whether the mandible ridges show phylogenetic signal with respect to the phylogeny published in Letsch et al. [38], we used the phylo.d function in the package 'caper' which is able to handle binary

coded characters and provides an estimate (D) for phylogenetic signal based on the sum of changes in estimated nodal values of the binary trait tested along the edges of the phylogeny. Additionally, probabilities are calculated for D resulting from no phylogenetic structure (phyl.sig), and whether D is based on Brownian motion (BM.sig) for each respective character.

Results

Mandible thickness and the variation of mandible shape and mandible ridges

The principle structure of the dragonfly mandible consists of two ball-and-socket articulations, a strongly sclerotized z-shaped mesal edge with four prominences and usually three distal incisivi (Figure 2). The mandibular orifice is broadly triangular in dorsal view. Thickness plots and external observation show that mandibles of all species have a system of up to six ridges, which are areas of thickened cuticle (Figure 2). Among these, the anterior and posterodorsal ones ("ADR" and "PDR") are present in all species and border the triangular mandibular orifice. The remaining four ridges are variable in location and thickness (Figure 2). If present, the anterior acetabular and the posterior condylar ridge ("AAR" and "PCR") run from the anterior and posterior articulation respectively towards the distal incisivi but end blindly well before they reach the distal area of the mandible (taxon dependent). Thickness plots also show that some mandibles, such as those of *Calopteryx*, *Epiophlebia*, *Tachopteryx* and some of the Aeshnidae and Libelluloidea, have anteriorly ridge-like areas at the same position as the ridges, but in fact these are just elevated curved regions only slightly thicker than the surrounding areas (Figure 2). We henceforth refer to these structures as “pseudoridges”, by contrast to “true” ridges that are thickened areas of the cuticle and show a thickness equal to the dorsal ridges. On the posterior side of the mandibles pseudoridges are more frequently encountered, with "true" ridges only present in *Onychogomphus*,

Cordulegastridae and *Neopetalia*. A mesal ridge, which is not visible externally, is present in all Libelluloidea studied (Figure 2). A lateral ridge, which originates at the attachment site of the mandibular abductor and extends half way to the apical incisivi in some species, is absent in *Calopteryx*, *Epiophlebia*, *Onychogomphus*, *Oligoaeschna*, *Anotogaster* and the Libellulidae studied. The lateral ridge is strongly developed in Petaluridae and in certain Gomphidae, but weakly developed in the rest of the species.

Principal component analysis (PCA) of mandible shape revealed four major components which together account for 68.38% of the shape variance (Figure 3). Phylogenetic signal could be detected in the shape data based on the multivariate K-statistic (Kmult = 0.68, P = 0.0001). Taxa that are represented by more than two species such as Libelluloidea, Aeshnidae and Gomphidae are separated from each other in the morphospace of most of the PC combinations. Petaluridae and Cordulegastridae are also separated in nearly all PC combinations, but these are only represented by two species each. The austropetaliid *Phylopetalia* is an outlier in nearly all PC combinations. The plot PC1 versus PC2 (Figure 3a) shows that the majority of shape variation along PC1 is related to the anterior mandibular joint (Landmark 13), the anterior dorsal ridge (L14) and the shape of the anterior acetabular (L15+16) and the lateral ridge (L17+18). With respect to the consensus shape, the anterior mandibular joint tends to be located more ventrally, while the anterior ridge is located more dorsally at the negative side of PC1. The anterior acetabular ridge is shorter and narrower and the lateral ridge is longer and wider while at the positive extreme of PC1 the situation is reversed. Along PC2, shape variation again relates to the anterior and posterior joints (L10+13) and to the anterior acetabular and the lateral ridge. PC2 mainly codes for the width of the ridges and the joints. Compared to all the above mentioned structures, the incisivi of the mandibles show only minor shape variations.

Mandible shape is not affected by size, strain ('MPDs'), JRFs or the MA based on the phylogenetic ANOVA (Table 3). With the exception of the median ridge which is a highly

conserved trait among Libelluloidea (D = -2.66; phyl.sig = 0.0001; BM.sig = 0.9879) the presence of mandibular ridges does not show phylogenetic signal (Table 3). Based on the Pagel [45] correlation test, the mandibular ridges also do not show pairwise correlations to each other (Table 3). The ADR and PDR ridges have not been included in this test since they are present in all taxa studied.

Mandible mechanics and the relation to shape and size

All mandibles show high strain directly at their distalmost tips where the bite force was applied, as well as at the attachment site of the large adductor muscle, which is always much thicker than the surrounding areas. Strain patterns differ between the anterior and posterior sides in each species with a generally higher strain (ε1 and ε3) on the posterior side. Compressive strains are higher in the lateral regions of the mandibles. A conspicuously thickened but externally indiscernible area lateroventral of the apical incisivi (Figure 2+4, e.g. Cordulegaster) shows high compressive strain (ε3) in most of the species. Areas of high tensile strain (ε1) are located medially between the apical incisivi and the mesal area and, depending on the species, laterally at the mesal base (Figure 4 and Figure S1).

While the thickness plots show that the presence and configuration of mandibular ridges and pseudoridges is highly variable, finite element analysis shows that strain distributions are not always related to ridge presence and location (Figure 4 and Figure S1). In Aeshnidae, the distribution of the most tensile strains (first principal strain, ε1) does not overlap with the areas where the anterior acetabular ridge and the lateral ridge are present. Also, there is a low overlap of ridge presence with strain patterns in Libelluloidea. For the most compressive principal strains at each point (ε3), Libelluloidea show no overlap of strain and structure for the prominent medial and lateral ridges.

In contrast to the thickness plots and strain distributions, box plot graphs of the median and overall variation in principal strain values for all mandibles (Figure 5) indicate a family

specific grouping for Libellulidae, Macromiidae and Gomphidae while median strain seems to be more variable in Cordulegastridae, Petaluridae and Aeshnidae. Although the application of a unit force of 1N to each mandible facilitates an easier comparison of strain patterns, for those species where bite forces could be measured [22,23] the box plots are also scaled in order to derive an estimate of the *in vivo* strain values. Results show that *Sympetrum* most likely experiences lower *in vivo* strain, whereas *Cordulegaster*, *Onychogomphus*, *Anax* and *Aeshna* have higher *in vivo* values, in the case of *Anax* and *Aeshna* nearly twice as high. Phylogenetic signal could not be detected in the strain data represented by the MPDs of each mandible based on the kappa statistic (K = 0.50, P = 0.3289).

Analysis of the joint mechanics expressed in terms of joint reaction force vectors (JRF) shows a similar family specific pattern like in the box plots of strain distributions for the angle between anterior and posterior JRFs in posterior view (α, Figure 6) while such a pattern is not apparent for the rest of the measured angles (β-η; Figure 6). The JRF angles α and β show phylogenetic signal (α: K = 0.91; p = 0.01; β: K = 0.89; p = 0.02; Table 3) while the distribution of the mandibular advantage does not show significant phylogenetic signal. JRF angles θ and η (the lateral "spread" of posterior and anterior JRF vectors, see Figure 6) show a correlation with mandible size (Table 3). The mean value of the mandible-closing mechanical advantage (MA) over all species is 0.38 ±0.017 with the lowest values (0.35) shown by species such as *Neopetalia* and *Phyllopetalia*. The highest MAs (0.41) are shown by *Aeshna* and *Sympetrum*. The MA is correlated with MPDs while the JRFs do not show such a correlation.

Discussion

The interplay of shape, biomechanics, phylogeny and size in dragonfly mandibles

Surprisingly few studies have tried to quantify mandible shape and biomechanics in insects [7,8,11,13] and there are no studies combining biomechanical determinants with shape

characteristics in a phylogenetic framework. Our results obtained from the 3D shape analysis and FEA of mandibles belonging to 21 different species of dragonflies suggest a rather complicated interplay of shape, biomechanics and phylogeny in taxa with uniform feeding habits. Mandible shape shows phylogenetic signal and the Kmult value lower than one suggests that taxa are more similar than expected under a Brownian motion model of evolution. This effect could also be detected for some biomechanical determinants (Table 3), specifically for the angle between anterior and posterior JRFs in anterior view (JRF α) and the direction of the posterior JRF in lateral view (JRF β). A possible explanation is selection of the above mentioned biomechanical factors to reach a certain mandible performance which in turn requires convergent evolution of a combination of shape variables supporting the required mechanical performance. In line with this suggestion is the correlation of the MA with MPDs (Table 3), since the MA is solely a shape dependent index of mandible performance. Furthermore, the results suggest that size effects only play a minor role for specific JRF angles although size differences are more than twofold (Table 2).

The lacking phylogenetic signal in MPDs despite such a signal in JRFs could be due to the averaging of strain results over a wide shape area. For a more detailed account it would be necessary to compare different strain *patterns* with each other and assess the phylogenetic signal in pattern variation. However, such an approach is obviously difficult to realize since this would require an exact structural similarity of each mandible so that a voxel-by-voxel comparison of strain values and subsequent correlation with shape voxels is possible.

Phylogenetic signal in a combination of shape and functional parameters has not been assessed so far in insects but is a well known phenomenon in vertebrates [46–51]. It was shown that multiple processes can in fact produce patterns of phenotypic diversification similar to phylogenetic signal [36,37,50,52,53]. In those instances where biomechanical determinants were additionally measured, the decisive influence of biomechanics on shape and vice versa was apparent [4,54–56] and in some instances superposing phylogenetic signal

[55]. Overall, our results suggest that the disparity in the phenotype is lower than expected under Brownian motion and biomechanics do not follow this pattern. In fact our results suggest that the biomechanical determinants measured here seem to be decoupled from the shape variation at this taxonomic level.

The mechanical advantage values measured for dragonflies are in the range of the most advantageous lever ratios (i.e. the most joint-near tooth row or advantageous muscle insertions) measured for vertebrates [57–59] and the American cockroach [8]. This relative uniformity of mechanical advantage in distantly related taxa such as cockroaches and dragonflies suggests that the observed differences in biomechanical determinants and shape obviously lead to a comparably narrow overall mandible performance space represented by the mechanical advantage. Taking into account the above mentioned decoupling of mechanics from shape, we suggest that this narrow MA range might be the effect of a "many-to-one mapping" of different forms to the same function [46,47,60] leading to the same functional performance space. However, more insect lineages need to be studied to corroborate this notion.

Biomechanical characteristics of dragonfly mandibles

Generally, higher strains are located around bite points and muscle attachments, as observed in similar FE studies of vertebrate crania and mandibles [61–63] and insect mandibles [64,65]. Another general area of high strain is located in all mandibles between the apical incisival area and the z-shaped mesal edge. Although it is currently not possible to reliably compare and test strain *patterns* against shape, we suggest that this correspondence in overall strain distribution is most probably related to the similarity in overall mandible morphology and applied loadings and constraints. Visual examination of the detailed strain patterns at the lateral parts of the mandibles, however, shows that the local strain distributions are highly variable. For example strain is not correlated with the presence of ridges in most of the

Aeshnidae and Libelluloidea studied. A similar phenomenon of non-correspondence of ridges with strain could be observed in vertebrates where the function of the brow ridge (supraorbital torus) in primates has been the subject of much debate, with studies showing that brow ridges are indeed lightly loaded during normal biting [66].

We applied a unit bite force (1N) to all mandibles because actual bite force values are not known for many of the rare species we investigated here. It should be remembered that absolute bite forces are not relevant for the purpose of this current study since strain patterns are of course independent of the absolute magnitude values of bite forces. On the other hand, the application of a standardized bite force allows an easy comparison of the relative mandible efficiencies. Our results suggest that the mandible shapes of Gomphidae and Macromiidae are among the most efficient in terms of principal strain distribution (Figure 5). Taking into account the bite forces which could be measured [22,23], the observed strain distributions for a unit force load are most likely an overestimation of *in vivo* strain in the smaller Libellulidae and *Calopteryx*, while they are an underestimation for the larger species within Aeshnidae, Cordulegastridae, Macromiidae, Petaluridae and to a lesser extend Gomphidae (Figure 4). As in vertebrates, absolute bite force in dragonflies likely depends on head geometry which also determines characteristics of the lever arm system such as e.g. adductor muscle mass and muscle architecture such as pennation and fibre length [59,69–71]. In contrast to vertebrates, however, an allometric scaling of bite force was not found for the species investigated here [22] which is also indicated by the lacking relationship between size and MPDs (Table 3). The middle sized gomphid *Onychogomphus forcipatus* showed an even higher bite force than one of the largest European dragonflies, *Cordulegaster bidentata* [22]. Future studies, taking into account more insect lineages, have to elucidate whether a non-allometric scaling of absolute bite forces is a more widespread phenomenon among insects.

A wider evolutionary perspective on mandible mechanics in basal insects

Strain levels at the posterior side of the mandibles are consistently higher than on the anterior sides (Figure 3) which is most probably related to the posteriorly directed force vector of the main mandibular adductor muscle. Interestingly, at the same time, the condyle-like mandibular part of the posterior joint shows a remarkable structural similarity within ectognathous insects (Bristletails, silverfish and winged insects) compared to the anterior joint although the food spectrum is highly variable [21,72–75]. Bristletails feed on algae, lichens and mosses, silverfish consume organic detritus and mayflies mainly feed on algae and detritus, with predacious species as the exception. A potential reason for this relative structural constancy in the posterior condyle may be the higher loadings this structure experiences compared to the anterior joint during biting. Structural change of the posterior mandibular joint during the evolution of the insect mandible might be restricted due to functional demands as was suggested for other animal groups [2,4,56]. In contrast, strain levels at the anterior mandibular joint are lower and this joint is at the same time structurally more variable throughout the early split ectognathous insects. Bristletails show a loose contact with the head capsule at the anterior part of the mandible [75], silverfish have a pincer-like structure guiding the mandible during movement in one direction [74,76], while mayflies show an anterior articulation complex in fact composed of two mandible-head contacts [77]. Finally, dragonflies and the majority of other chewing-biting insects e.g. Polyneoptera show the typical ball-and-socket joint type at the anterior side of the mandible. This structural variability in the anterior mandible joint during early insect evolution might have been possible due to the lower loadings experienced so that the constraining effect of biomechanics on shape was lower. However, biomechanical data for bristletails, silverfish and mayflies will be needed to test these ideas in an evolutive framework. Since sensitivity studies have proven the significant negative impact of simplifications in geometry and boundary conditions for vertebrates [69,78–89], much more experimental data on insect mouthpart mechanics is needed to quantitatively assess patterns of biomechanical evolution across insects.

Acknowledgements

We thank Anke Schmitz for help during the nano-indentation experiments and Felix Beckmann, Karen Meusemann, Björn M. von Reumont and Susanne Düngelhoef for help during the SRµCT experiments. Sina David and Johannes Funken (German Sport University, Cologne) are sincerely thanked for their help during bite force measurements. Manon Galland (currently University College Dublin, Dublin) helped with the geometric morphometric analysis workflow. Bernhard Misof and Anthony Herrel are thanked for valuable discussions during the preparation of this manuscript. We furthermore thank the very constructive comments of four reviewers to an earlier version of the manuscript.

Competing interests

We have no competing interests

Author contributions

AB and MJF conceived and designed the study. AB and AP did the SRµCT, AB and HS did the nano-indentations. HD helped with the FEA. AB analysed and interpreted the data. All authors read and corrected earlier versions of the manuscript and approved the final version.

Funding

The financial support of the Deutsches Elektronen-Synchrotron (DESY: I-20120065) and the Paul-Scherrer Institut (PSI: 20150464) to perform synchrotron experiments is gratefully acknowledged. AB was supported by a research fellowship of the Deutsche Forschungsgemeinschaft (DFG: BL 1355/1-1). HD was supported through BBSRC grant BB/M008525/1.

References

1. Gould, S. J. 1966 Allometry and Size in Ontogeny and Phylogeny. *Biol. Rev.* 41, 587–638. (doi:10.1111/j.1469-185X.1966.tb01624.x)

2. Smith, J. M., Burian, R., Kauffman, S., Alberch, P., Campbell, J., Goodwin, B., Lande, R., Raup, D. & Wolpert, L. 1985 Developmental Constraints and Evolution: A Perspective from the Mountain Lake Conference on Development and Evolution. *Q. Rev. Biol.* 60, 265–287.

3. Gans, C. 1988 On phylogenetic constraints. *Acta Morphol. Neerl. Scand.* 27, 133–138.

4. Arnold, S. J. 1992 Constraints on Phenotypic Evolution. *Am. Nat.* 140, S85–S107.

5. Paul, J. & Gronenberg, W. 1999 Optimizing force and velocity: mandible muscle fibre attachments in ants. *J. Exp. Biol.* 202 (Pt 7), 797–808.

6. Goyens, J., Dirckx, J., Dierick, M., Hoorebeke, L. V. & Aerts, P. 2014 Biomechanical determinants of bite force dimorphism in Cyclommatus metallifer stag beetles. *J. Exp. Biol.* 217, 1065–1071. (doi:10.1242/jeb.091744)

7. Schmitt, C., Rack, A. & Betz, O. 2014 Analyses of the mouthpart kinematics in Periplaneta americana (Blattodea, Blattidae) by using Synchrotron-based X-ray cineradiography. *J. Exp. Biol.* , jeb.092742. (doi:10.1242/jeb.092742)

8. Weihmann, T., Reinhardt, L., Weißing, K., Siebert, T. & Wipfler, B. 2015 Fast and Powerful: Biomechanics and Bite Forces of the Mandibles in the American Cockroach *Periplaneta americana*. *PLoS ONE* 10, e0141226. (doi:10.1371/journal.pone.0141226)

9. Josephson, R. K. & Young, D. 1987 Fiber Ultrastructure and Contraction Kinetics in Insect Fast Muscles. *Am. Zool.* 27, 991–1000. (doi:10.1093/icb/27.4.991)

10. Gronenberg, W., Paul, J., Just, S. & Hölldobler, B. 1997 Mandible muscle fibers in ants: fast or powerful? *Cell Tissue Res.* 289, 347–361.

11. Paul, J. 2001 Mandible movements in ants. *Comp. Biochem. Physiol. A. Mol. Integr. Physiol.* 131, 7–20.

12. Paul, J. & Gronenberg, W. 2002 Motor control of the mandible closer muscle in ants. *J. Insect Physiol.* 48, 255–267.

13. Gorb, S. & Beutel, R. G. 2000 Head-capsule design and mandible control in beetle larvae: a three-dimensional approach. *J. Morphol.* 244, 1–14. (doi:10.1002/(SICI)1097-4687(200004)244:1<1::AID-JMOR1>3.0.CO;2-E)

14. Smith, T. R. & Capinera, J. L. 2005 Mandibular Morphology of Some Floridian Grasshoppers (Orthoptera: Acrididae). *Fla. Entomol.* 88, 204–207.

15. Matsuda, R. 1965 Morphology and evolution of the insect head. *Mem. Am. Entomol. Inst.* 1, 1–334.

16. Labandeira, C. C. 1997 Insect Mouthparts: Ascertaining the Paleobiology of Insect Feeding Strategies. *Annu. Rev. Ecol. Syst.* 28, 153–193.

17. Grimaldi, D. & Engel, M. S. 2005 *Evolution of the Insects*. Cambridge University Press.

18. Corbet, P. S. 1999 Dragonflies: behaviour and ecology of Odonata. , xxxii + 829 pp.

19. Tillyard, R. J. 1917 *The biology of dragonflies (Odonata or Paraneuroptera)*. Cambridge, United Kingdom.

20. Asahina, S. 1954 Morphological study of a relic dragonfly Epiophlebia superstes Selys (Odonata, Anisozygoptera). *Jpn. Soc. Promot. Sci.* , 153p.

21. Beutel, R. G., Friedrich, F., Ge, S. Q. & Yang, X. K. 2014 *Insect Morphology and Phylogeny*. Berlin: De Gruyter.

22. David, S., Funken, J., Potthast, W. & Blanke, A. 2016 Musculoskeletal modelling under an evolutionary perspective: deciphering the role of single muscle regions in closely related insects. *J. R. Soc. Interface* 13, 20160675. (doi:10.1098/rsif.2016.0675)

23. David, S., Funken, J., Potthast, W. & Blanke, A. 2016 Musculoskeletal modeling of the dragonfly mandible system as an aid to understanding the role of single muscles in an evolutionary context. *J. Exp. Biol.* , jeb.132399. (doi:10.1242/jeb.132399)

24. Klocke, D. & Schmitz, H. 2011 Water as a major modulator of the mechanical properties of insect cuticle. *Acta Biomater.* 7, 2935–2942. (doi:10.1016/j.actbio.2011.04.004)

25. Klocke, D. & Schmitz, H. 2012 Material properties of photomechanical infrared receptors in pyrophilous Melanophila beetles and Aradus bugs. *Acta Biomater.* 8, 3392–3399. (doi:10.1016/j.actbio.2012.05.020)

26. Oliver, W. C. & Pharr, G. M. 1992 An improved technique for determining hardness and elastic modulus using load and displacement sensing indentation experiments. *J. Mater. Res.* 7, 1564–1583. (doi:10.1557/JMR.1992.1564)

27. Romeis, B. 1989 *Mikroskopische Technik*. München: Urban & Schwarzenberg.

28. Beckmann, F., Herzen, J., Haibel, A., Müller, B. & Schreyer, A. 2008 High density resolution in synchrotron-radiation-based attenuation-contrast microtomography. *Proc. SPIE* 7078, 70781D–70781D–13. (doi:10.1117/12.794617)

29. Stampanoni, M., Marone, F., Modregger, P., Pinzer, B., Thüring, T., Vila‐Comamala, J., David, C. & Mokso, R. 2010 Tomographic hard X‐ray phase contrast micro‐ and nano‐imaging at TOMCAT. *AIP Conf. Proc.* 1266, 13–17. (doi:10.1063/1.3478189)

30. Blanke, A., Greve, C., Mokso, R., Beckmann, F. & Misof, B. 2013 An updated phylogeny of Anisoptera including formal convergence analysis of morphological characters. *Syst. Entomol.* 38, 474–490. (doi:10.1111/syen.12012)

31. Yushkevich, P. A., Piven, J., Hazlett, H. C., Smith, R. G., Ho, S., Gee, J. C. & Gerig, G. 2006 User-guided 3D active contour segmentation of anatomical structures:

significantly improved efficiency and reliability. *NeuroImage* 31, 1116–1128. (doi:10.1016/j.neuroimage.2006.01.015)

32. Westneat, M. W. 1995 Feeding, Function, and Phylogeny: Analysis of Historical Biomechanics in Labrid Fishes Using Comparative Methods. *Syst. Biol.* 44, 361–383. (doi:10.1093/sysbio/44.3.361)

33. Anderson, P. S. L., Friedman, M., Brazeau, M. D. & Rayfield, E. J. 2011 Initial radiation of jaws demonstrated stability despite faunal and environmental change. *Nature* 476, 206–209. (doi:10.1038/nature10207)

34. Hulsey, C. D. & Wainwright, P. C. 2002 Projecting mechanics into morphospace: disparity in the feeding system of labrid fishes. *Proc. Biol. Sci.* 269, 317–326. (doi:10.1098/rspb.2001.1874)

35. Anderson, P. S. L. 2009 Biomechanics, functional patterns, and disparity in Late Devonian arthrodires. *Paleobiology* 35, 321–342. (doi:10.1666/0094-8373-35.3.321)

36. Adams, D. C. 2014 A Generalized K Statistic for Estimating Phylogenetic Signal from Shape and Other High-Dimensional Multivariate Data. *Syst. Biol.* , syu030. (doi:10.1093/sysbio/syu030)

37. Blomberg, S. P., Garland, T. & Ives, A. R. 2003 Testing for Phylogenetic Signal in Comparative Data: Behavioral Traits Are More Labile. *Evolution* 57, 717–745. (doi:10.1111/j.0014-3820.2003.tb00285.x)

38. Letsch, H., Gottsberger, B. & Ware, J. L. 2016 Not going with the flow: a comprehensive time-calibrated phylogeny of dragonflies (Anisoptera: Odonata: Insecta) provides evidence for the role of lentic habitats on diversification. *Mol. Ecol.* , n/a-n/a. (doi:10.1111/mec.13562)

39. Revell, L. J. 2012 phytools: an R package for phylogenetic comparative biology (and other things). *Methods Ecol. Evol.* 3, 217–223. (doi:10.1111/j.2041-210X.2011.00169.x)

40. Adams, D. C. & Otárola-Castillo, E. 2013 geomorph: an r package for the collection and analysis of geometric morphometric shape data. *Methods Ecol. Evol.* 4, 393–399. (doi:10.1111/2041-210X.12035)

41. Dryden, I. L. 2015 Shapes package. *R Found. Stat. Comput. Vienna Austria Contrib. Package Version 11-11 URL HttpwwwR-Proj.*

42. Popescu, A.-A., Huber, K. T. & Paradis, E. 2012 ape 3.0: New tools for distance-based phylogenetics and evolutionary analysis in R. *Bioinforma. Oxf. Engl.* 28, 1536–1537. (doi:10.1093/bioinformatics/bts184)

43. Gower, J. C. 1975 Generalized procrustes analysis. *Psychometrika* 40, 33–51. (doi:10.1007/BF02291478)

44. Rohlf, F. J. & Slice, D. 1990 Extensions of the Procrustes Method for the Optimal Superimposition of Landmarks. *Syst. Zool.* 39, 40–59. (doi:10.2307/2992207)

45. Pagel, M. 1994 Detecting Correlated Evolution on Phylogenies: A General Method for the Comparative Analysis of Discrete Characters. *Proc. R. Soc. Lond. B Biol. Sci.* 255, 37–45. (doi:10.1098/rspb.1994.0006)

46. Alfaro, M. E., Bolnick, D. I. & Wainwright, P. C. 2005 Evolutionary consequences of many-to-one mapping of jaw morphology to mechanics in labrid fishes. *Am. Nat.* 165, E140-154. (doi:10.1086/429564)

47. Wainwright, P. C., Alfaro, M. E., Bolnick, D. I. & Hulsey, C. D. 2005 Many-to-One Mapping of Form to Function: A General Principle in Organismal Design? *Integr. Comp. Biol.* 45, 256–262. (doi:10.1093/icb/45.2.256)

48. Rezende, E. L. & Diniz-Filho, J. A. F. 2012 Phylogenetic analyses: comparing species to infer adaptations and physiological mechanisms. *Compr. Physiol.* 2, 639–674. (doi:10.1002/cphy.c100079)

49. Rheindt, F. E., Grafe, * T. Ulmar & Abouheif‡, E. 2004 Rapidly evolving traits and the comparative method: how important is testing for phylogenetic signal? *Evol. Ecol. Res.* 6, 377–396.

50. Revell, L. J., Harmon, L. J. & Collar, D. C. 2008 Phylogenetic Signal, Evolutionary Process, and Rate. *Syst. Biol.* 57, 591–601. (doi:10.1080/10635150802302427)

51. Segall, M., Cornette, R., Fabre, A.-C., Godoy-Diana, R. & Herrel, A. 2016 Does aquatic foraging impact head shape evolution in snakes? *Proc R Soc B* 283, 20161645. (doi:10.1098/rspb.2016.1645)

52. Ackerly, D. 2009 Conservatism and diversification of plant functional traits: Evolutionary rates versus phylogenetic signal. *Proc. Natl. Acad. Sci. U. S. A.* 106, 19699–19706. (doi:10.1073/pnas.0901635106)

53. Pennell, M. W. & Harmon, L. J. 2013 An integrative view of phylogenetic comparative methods: connections to population genetics, community ecology, and paleobiology. *Ann. N. Y. Acad. Sci.* 1289, 90–105. (doi:10.1111/nyas.12157)

54. Levinton, J. S. & Allen, B. J. 2005 The paradox of the weakening combatant: trade-off between closing force and gripping speed in a sexually selected combat structure. *Funct. Ecol.* 19, 159–165. (doi:10.1111/j.0269-8463.2005.00968.x)

55. Piras, P., Maiorino, L., Teresi, L., Meloro, C., Lucci, F., Kotsakis, T. & Raia, P. 2013 Bite of the Cats: Relationships between Functional Integration and Mechanical Performance as Revealed by Mandible Geometry. *Syst. Biol.* 62, 878–900. (doi:10.1093/sysbio/syt053)

56. Konuma, J. & Chiba, S. 2007 Trade-offs between force and fit: extreme morphologies associated with feeding behavior in carabid beetles. *Am. Nat.* 170, 90–100. (doi:10.1086/518182)

57. Sakamoto, M. 2010 Jaw biomechanics and the evolution of biting performance in theropod dinosaurs. *Proc. R. Soc. Lond. B Biol. Sci.* , rspb20100794. (doi:10.1098/rspb.2010.0794)

58. Dutel, H., Herbin, M., Clément, G. & Herrel, A. 2015 Bite force in the extant coelacanth latimeria: the role of the intracranial joint and the basicranial muscle. *Curr. Biol. CB* 25, 1228–1233. (doi:10.1016/j.cub.2015.02.076)

59. McIntosh, A. F. & Cox, P. G. 2016 Functional implications of craniomandibular morphology in African mole-rats (Rodentia: Bathyergidae). *Biol. J. Linn. Soc.* 117, 447–462. (doi:10.1111/bij.12691)

60. Alfaro, M. E., Bolnick, D. I. & Wainwright, P. C. 2004 Evolutionary Dynamics of Complex Biomechanical Systems: An Example Using the Four-Bar Mechanism. *Evolution* 58, 495–503. (doi:10.1111/j.0014-3820.2004.tb01673.x)

61. Fitton, L. C., Shi, J. F., Fagan, M. J. & O'Higgins, P. 2012 Masticatory loadings and cranial deformation in Macaca fascicularis: a finite element analysis sensitivity study. *J. Anat.* 221, 55–68. (doi:10.1111/j.1469-7580.2012.01516.x)

62. Curtis, N., Jones, M. E. H., Evans, S. E., O'Higgins, P. & Fagan, M. J. 2013 Cranial sutures work collectively to distribute strain throughout the reptile skull. *J. R. Soc. Interface* 10, 20130442. (doi:10.1098/rsif.2013.0442)

63. Gill, P. G., Purnell, M. A., Crumpton, N., Brown, K. R., Gostling, N. J., Stampanoni, M. & Rayfield, E. J. 2014 Dietary specializations and diversity in feeding ecology of the earliest stem mammals. *Nature* 512, 303–305. (doi:10.1038/nature13622)

64. Hörnschemeyer, T., Bond, J. & Young, P. G. 2013 Analysis of the functional morphology of mouthparts of the beetle *Priacma serrata*, and a discussion of possible food sources. *J. Insect Sci.* 13, 1–14. (doi:10.1673/031.013.12601)

65. Goyens, J., Soons, J., Aerts, P. & Dirckx, J. 2014 Finite-element modelling reveals force modulation of jaw adductors in stag beetles. *J. R. Soc. Interface* 11, 20140908. (doi:10.1098/rsif.2014.0908)

66. Kupczik, K., Dobson, C. a., Crompton, R. h., Phillips, R., Oxnard, C. e., Fagan, M. j. & O'Higgins, P. 2009 Masticatory loading and bone adaptation in the supraorbital torus of developing macaques. *Am. J. Phys. Anthropol.* 139, 193–203. (doi:10.1002/ajpa.20972)

67. Strait, D. S. et al. 2010 The Structural Rigidity of the Cranium of Australopithecus africanus: Implications for Diet, Dietary Adaptations, and the Allometry of Feeding Biomechanics. *Anat. Rec. Adv. Integr. Anat. Evol. Biol.* 293, 583–593. (doi:10.1002/ar.21122)

68. Ross, C. F., Berthaume, M. A., Dechow, P. C., Iriarte-Diaz, J., Porro, L. B., Richmond, B. G., Spencer, M. & Strait, D. 2011 In vivo bone strain and finite-element modeling of the craniofacial haft in catarrhine primates. *J. Anat.* 218, 112–141. (doi:10.1111/j.1469-7580.2010.01322.x)

69. Gröning, F., Jones, M. E. H., Curtis, N., Herrel, A., O'Higgins, P., Evans, S. E. & Fagan, M. J. 2013 The importance of accurate muscle modelling for biomechanical analyses: a case study with a lizard skull. *J. R. Soc. Interface* 10, 20130216. (doi:10.1098/rsif.2013.0216)

70. Cox, P. G. & Baverstock, H. 2015 Masticatory Muscle Anatomy and Feeding Efficiency of the American Beaver, Castor canadensis (Rodentia, Castoridae). *J. Mamm. Evol.* , 1–10. (doi:10.1007/s10914-015-9306-9)

71. Ledogar, J. A. et al. 2016 Mechanical evidence that Australopithecus sediba was limited in its ability to eat hard foods. *Nat. Commun.* 7, 10596. (doi:10.1038/ncomms10596)

72. Engel, M. S. & Grimaldi, D. A. 2004 New light shed on the oldest insect. *Nature* 427, 627–630. (doi:10.1038/nature02291)

73. Blanke, A., Wipfler, B., Letsch, H., Koch, M., Beckmann, F., Beutel, R. & Misof, B. 2012 Revival of Palaeoptera—head characters support a monophyletic origin of

Odonata and Ephemeroptera (Insecta). *Cladistics* 28, 560–581. (doi:10.1111/j.1096-0031.2012.00405.x)

74. Blanke, A., Koch, M., Wipfler, B., Wilde, F. & Misof, B. 2014 Head morphology of *Tricholepidion gertschi* indicates monophyletic Zygentoma. *Front. Zool.* 11, 16. (doi:10.1186/1742-9994-11-16)

75. Blanke, A., Machida, R., Szucsich, N. U., Wilde, F. & Misof, B. 2015 Mandibles with two joints evolved much earlier in the history of insects: dicondyly is a synapomorphy of bristletails, silverfish and winged insects. *Syst. Entomol.* 40, 357–364. (doi:10.1111/syen.12107)

76. Lieven, A. F. von 2000 The transformation from monocondylous to dicondylous mandibles in the Insecta. *Zool. Anz.* 239, 139–146.

77. Staniczek, A. H. 2000 The mandible of silverfish (Insecta: Zygentoma) and mayflies (Ephemeroptera): its morphology and phylogenetic significance. *Zool. Anz.* 239, 147–178.

78. Gröning, F., Bright, J. A., Fagan, M. J. & O'Higgins, P. 2012 Improving the validation of finite element models with quantitative full-field strain comparisons. *J. Biomech.* 45, 1498–1506. (doi:10.1016/j.jbiomech.2012.02.009)

79. Gröning, F., Fagan, M. & O'higgins, P. 2012 Modeling the human mandible under masticatory loads: Which input variables are important? *Anat. Rec. Adv. Integr. Anat. Evol. Biol.* 295, 853–863. (doi:10.1002/ar.22455)

80. Gröning, F. & Fagan, M. J. 2012 Comment on 'The effects of modelling simplifications on craniofacial finite element models: The alveoli (tooth sockets) and periodontal ligaments' (volume 44, issue 10, pages 1831–1838). *J. Biomech.* 45, 1749–1750. (doi:10.1016/j.jbiomech.2011.10.042)

81. Bright, J. A. & Gröning, F. 2011 Strain accommodation in the zygomatic arch of the pig: A validation study using digital speckle pattern interferometry and finite element analysis. *J. Morphol.* 272, 1388–1398. (doi:10.1002/jmor.10991)

82. Curtis, N., Jones, M. E. H., Lappin, A. K., O'Higgins, P., Evans, S. E. & Fagan, M. J. 2010 Comparison between in vivo and theoretical bite performance: Using multi-body modelling to predict muscle and bite forces in a reptile skull. *J. Biomech.* 43, 2804–2809. (doi:10.1016/j.jbiomech.2010.05.037)

83. Curtis, N., Jones, M. E. H., Evans, S. E., Shi, J., O'Higgins, P. & Fagan, M. J. 2010 Predicting muscle activation patterns from motion and anatomy: modelling the skull of Sphenodon (Diapsida: Rhynchocephalia). *J. R. Soc. Interface R. Soc.* 7, 153–160. (doi:10.1098/rsif.2009.0139)

84. Charles, J. P., Cappellari, O., Spence, A. J., Wells, D. J. & Hutchinson, J. R. 2016 Muscle moment arms and sensitivity analysis of a mouse hindlimb musculoskeletal model. *J. Anat.* 229, 514–535. (doi:10.1111/joa.12461)

85. Kupczik, K., Dobson, C. A., Fagan, M. J., Crompton, R. H., Oxnard, C. E. & O'Higgins, P. 2007 Assessing mechanical function of the zygomatic region in macaques: validation and sensitivity testing of finite element models. *J. Anat.* 210, 41–53. (doi:10.1111/j.1469-7580.2006.00662.x)

86. Sellers, W. I. & Crompton, R. H. 2004 Using sensitivity analysis to validate the predictions of a biomechanical model of bite forces. *Ann. Anat. - Anat. Anz.* 186, 89–95. (doi:10.1016/S0940-9602(04)80132-8)

87. Toro-Ibacache, V., Fitton, L. C., Fagan, M. J. & O'Higgins, P. 2016 Validity and sensitivity of a human cranial finite element model: implications for comparative studies of biting performance. *J. Anat.* 228, 70–84. (doi:10.1111/joa.12384)

88. Tseng, Z. J., Mcnitt-Gray, J. L., Flashner, H., Wang, X. & Enciso, R. 2011 Model Sensitivity and Use of the Comparative Finite Element Method in Mammalian Jaw Mechanics: Mandible Performance in the Gray Wolf. *PLoS ONE* 6, e19171. (doi:10.1371/journal.pone.0019171)

89. Watson, P. J., Fagan, M. J. & Dobson, C. A. 2015 Sensitivity to model geometry in finite element analyses of reconstructed skeletal structures: Experience with a juvenile pelvis. *Proc. Inst. Mech. Eng. [H]* 229, 9–19. (doi:10.1177/0954411914564476)

Tables

Table 1 Landmark definitions used to characterize shape variation in the dragonfly mandible.

Table 2 Taxon sampling used and overview of head sizes and mandible ridge presence. AAR, anterior acetabular ridge; PCR, posterior condylar ridge; MR, median ridge; LR, lateral ridge.

Table 3 Statistical testing framework to test the influence of shape, size, biomechanical determinants and trait presence on each other and to test phylogenetic signal. PC, principal component; AAR, anterior acetabular ridge; PCR, posterior condylar ridge; MR, median ridge; LR, lateral ridge, JRF, joint reaction force. For the definition of JRF angles please refer to Figure 6.

Figures

Figure 1 (a) Lateral section through the mandible of Onychogomphus forcipatus to show the location of the posterior (PR) and anterior (AR) dorsal ridges. (b) **3D representation of a**

dragonfly mandible in lateral view to show the position of the landmarks (red dots) and semilandmarks (orange), the joints (asterisks), muscle force and bite force, and joint tip triangle (blue). Circles represent landmarks which are on the backside of the mandible.

Figure 2 (a) Overview of the head of *Onychogomphus forcipatus* (Gomphidae) in lateral view showing the location of the mandibles within the head and the axis of rotation generated by the anterior and posterior mandibular joints. **(b) Dimensionless thickness plots for representatives of all dragonfly families.** Blue areas represent the thinnest regions, and red areas the thickest. Black and blue arrows indicate ridges and pseudoridges mentioned in the text, asterisks indicate the location of joints. Note the appearance of a mesal ridge (MR) in all Libelluloidea studied. Left column, anterior view; Middle column, lateral view; Right column, posterior view. Left column arrow: Anterior acetabular (pseudo)ridge; middle column: Lateral ridge; Right column: Posterior condylar (pseudo)ridge. Blue arrows indicate locations of the anterior and posterior dorsal ridges enframing the mandibular orifice. Abbreviations: ADR, anterior dorsal ridge; ama, anterior mandibular articulation; inc, incisival area; ma, mesal area; PDR, posterior dorsal ridge; pma, posterior mandibular articulation. Mandible joints are aligned to each other so that the virtual axis of rotation of the mandible points perpendicular out of the figure. Mandibles not to scale.

Figure 3 Principal component analysis showing all combinations of the first four mandible shape components. Data point acronyms are the first four letters of species names (see Table 2), semi-transparent polygon boxes relate to higher taxa. Mandible images show the plots of the landmark vectors for the extreme mandible shapes of PC1 and PC2.

Figure 4 First (ε1) and third (ε3) principal strain distributions in the mandibles mapped onto the most recent comprehensive phylogeny provided for dragonflies (Anisoptera;

Letsch et al. [38]). Left column, anterior view; middle column, lateromedial view; right column, posterior view; ε1 upper row with left-hand colour legend; ε3 lower row with right hand legend. A unit force of 1N was used for all species. Only exemplary mandibles are shown, for a full overview of strain patterns per species please refer to Figure S1.

Figure 5 Boxplots showing the range of first (ε1, right side) and third (ε3, left side) principal strain distributions for the middle part of each mandible (see sample insert) of the full species set at a unit force of 1N. Note that the highlighted middle part was used to calculate the median of the 1000 nodes showing the highest displacements (MPDs, "median peak displacements"). Coloured boxes indicate families, red boxplots show ranges of ε1 and ε3 after rescaling according to the bite force measurements. Please refer to figure S2 for an overview of strain ranges including outliers.

Figure 6 The range of joint reaction force (JRF) vectors for anisopteran mandibles. (a-d) Visual overview of measured angles. The dashed line shows the virtual joint axis around which the mandible rotates during biting. All mandibles were aligned to this axis for comparison of JRFs. (b) The range of aligned JRF vectors in posterior view, (c) in lateral view, and (d) in ventral view (seen along the triangle plane indicated in (a). (e) Overview of the measured angles, coloured boxes indicate families with the same colour code as in figure 3. See online 3D models in S3 for fully interactive 3D models of joint-tip-triangles.

Supplementary online material

Supplementary online figure S1 Results of nano-indentation material testing of five species of dragonflies and additonal overview of strain patterns for the full taxon sampling used in this study.

Supplementary online figure S2 Full boxplots including outliers showing the range of ε1 and ε3 distributions for each species. The order of boxplots is the same like in the main text.

Supplementary online 3D model S3 Three dimensional models of the joint-tip triangles used for the description of joint reaction forces. Triangles are labeled according to species, length of lines corresponds to the size of the vector. Note that the depicted model is a low resolution model not used in the finite-element analyses. Please download the freeware Blender (www.blender.org) in order to open the file with the full functionality.

family	species	HW [mm]	AAR	PCR	MR	LR
Zygoptera	*C. splendens*	6.12	0	0	0	0
Epiophlebiidae	*E. superstes*	7.72	0	0	0	0
Gomphidae	*O. forcipatus*	9.70	1	1	0	0
Gomphidae	*H. brevistylus*	10.55	1	0	0	1
Gomphidae	*Z. batesi*	9.59	1	0	0	1
Petaluridae	*P. raptor*	11.61	1	0	0	1
Petaluridae	*T. thoreyi*	10.90	0	0	0	1
Aeshnidae	*A. imperator*	9.88	1	0	0	0
Aeshnidae	*A. mixta*	8.38	1	0	0	1
Aeshnidae	*A. anisoptera*	10.69	1	0	0	1
Aeshnidae	*A. isoceles*	9.61	0	1	0	0
Aeshnidae	*O. pryeri*	8.53	0	0	0	0
Austropetaliidae	*P. apicalis*	9.74	0	0	0	0
Cordulegastridae	*A. sieboldii*	12.57	1	1	0	0
Cordulegastridae	*C. bidentata*	8.69	1	1	0	0
Neopetaliidae	*N. punctata*	8.97	0	1	0	0
Libelluloidea	*M. taeniolata*	10.00	1	0	1	1
Libelluloidea	*E. elegans*	10.78	0	0	1	1
Libelluloidea	*C. aenea*	8.12	1	0	1	1
Libelluloidea	*S. vulgatum*	5.22	0	0	1	0
Libelluloidea	*L. depressa*	8.21	0	0	1	0

	Tested traits	K	p-value
Kappa	JRF (α)	0.91	**0.0127**
	JRF (β)	0.89	**0.0185**
	JRF (γ)	0.57	0.2133
	JRF (δ)	0.55	0.2460
	JRF (θ)	0.26	0.9054
	JRF (η)	0.29	0.8175
	MA	0.66	0.1059

		R^2	p-value
Procrustes PGLS	Shape vs. Size	0.0758	0.7373
	Shape vs. MPDs	0.0702	0.5726
	Shape vs. JRF (α)	0.0432	0.7568
	Shape vs. JRF (β)	0.0424	0.5351
	Shape vs. JRF (γ)	0.1430	0.2442
	Shape vs. JRF (δ)	0.1246	0.2523
	Shape vs. JRF (θ)	0.0640	0.9732
	Shape vs. JRF (η)	0.1070	0.8429
	Shape vs. MA	0.0762	0.0904
PIC	Size vs. MPDs	0.0927	0.0972
	JRF (α) vs. MPDs	0.0005	0.9222
	JRF (β) vs. MPDs	0.0328	0.4319
	JRF (γ) vs. MPDs	0.0598	0.2854
	JRF (δ) vs. MPDs	0.0010	0.8900
	JRF (θ) vs. MPDs	0.1281	0.1112
	JRF (η) vs. MPDs	0.1021	0.1580
	MA vs. MPDs	**0.3439**	**0.0052**
	JRF (α) vs. size	0.0504	0.3280
	JRF (β) vs. Size	0.0143	0.6063
	JRF (γ) vs. Size	0.0714	0.2417
	JRF (δ) vs. Size	0.0710	0.2431
	JRF (θ) vs. Size	**0.2739**	**0.0149**
	JRF (η) vs. Size	**0.3836**	**0.0028**
	MA vs. Size	0.1625	0.0700

		est. D	no phyl.sig (BM.sig)
Phyl. sig. ridge presence	AAR	0.67	0.27 (0.21)
	PCR	-0.32	0.06 (0.65)
	MR	**-2.74**	**1 (0.02)**
	LR	0.78	0.33 (0.16)

		likelihood-ratio	p-value
Pairwise corr. of ridges	AAR | PCR	2.1031	0.7168
	AAR | MR	0.9736	0.9138
	AAR | LR	5.8201	0.2138
	PCR | MR	2.6425	0.4742
	PCR | LR	6.0530	0.1945
	MR | LR	1.4166	0.8413

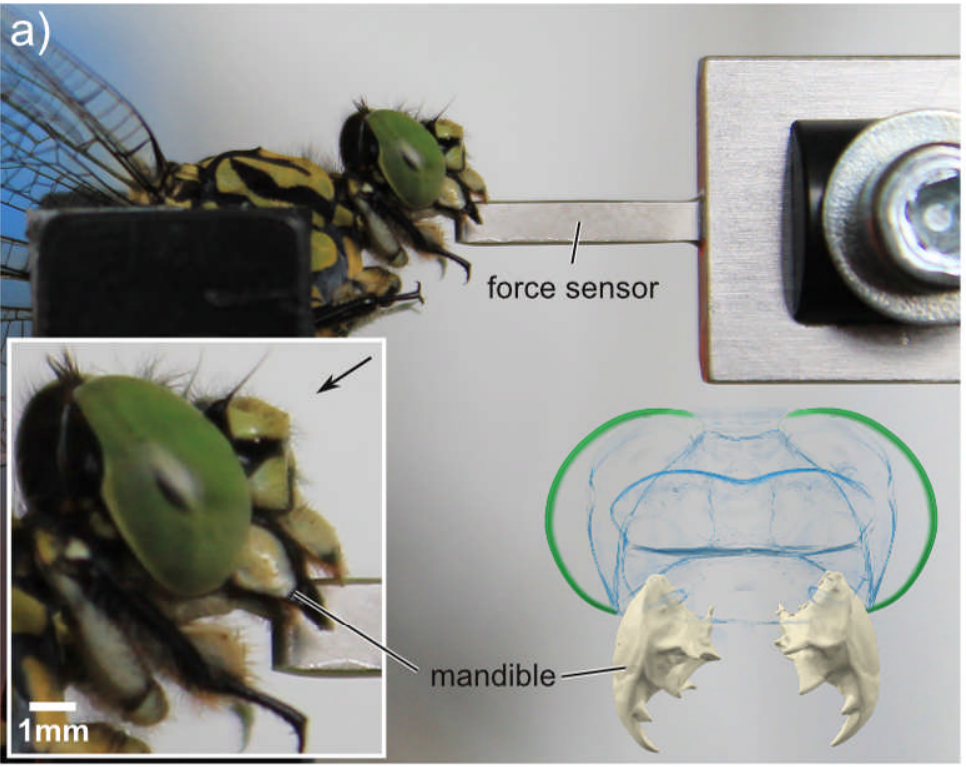
a)
force sensor
mandible
1mm

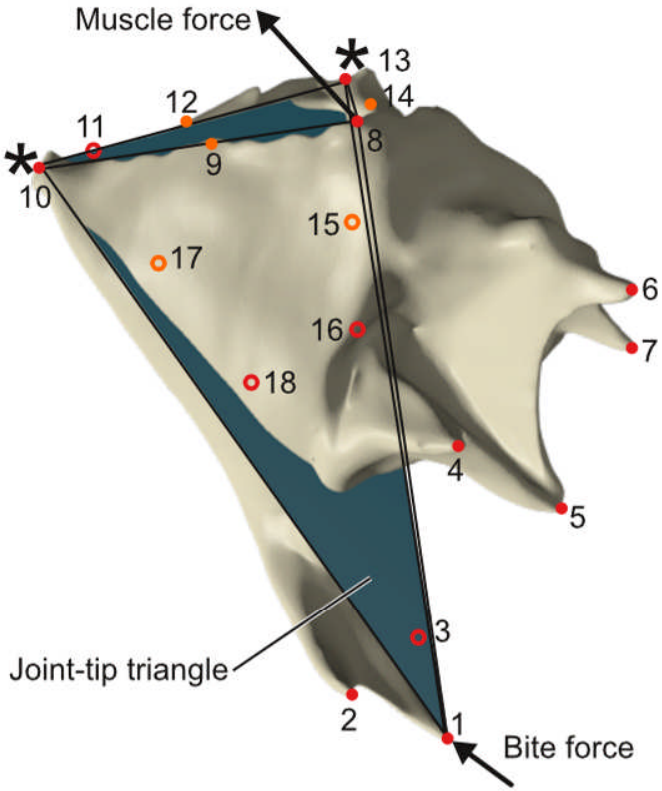
b)
Muscle force
Joint-tip triangle
Bite force
1
2
3
4
5
6
7
8
9
10
11
12
13
14
15
16
17
18

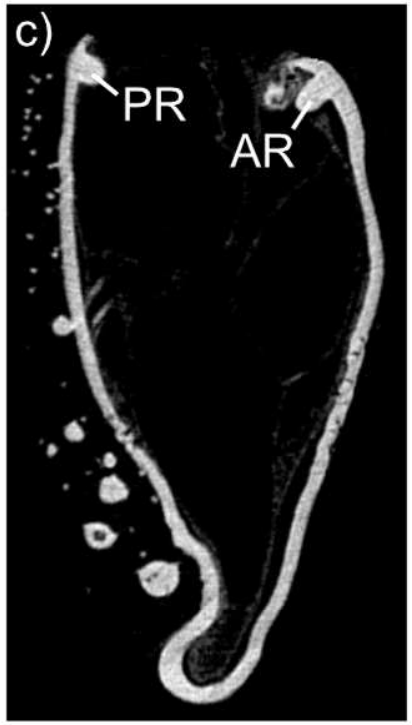
c)
PR
AR

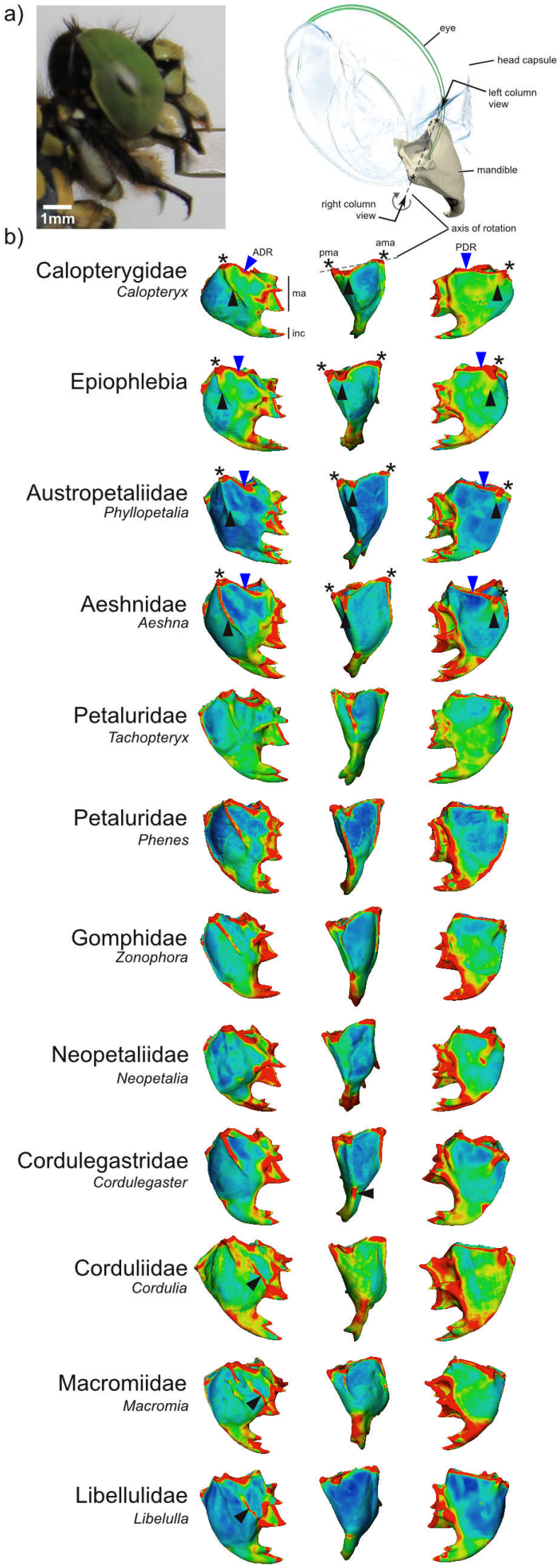
a)
1mm
eye
head capsule
left column view
mandible
right column view
axis of rotation
b)
ADR
pma
ama
PDR
ma
inc
Calopterygidae
Calopteryx
Epiophlebia
Austropetaliidae
Phyllopetalia
Aeshnidae
Aeshna
Petaluridae
Tachopteryx
Petaluridae
Phenes
Gomphidae
Zonophora
Neopetaliidae
Neopetalia
Cordulegastridae
Cordulegaster
Corduliidae
Cordulia
Macromiidae
Macromia
Libellulidae
Libelulla

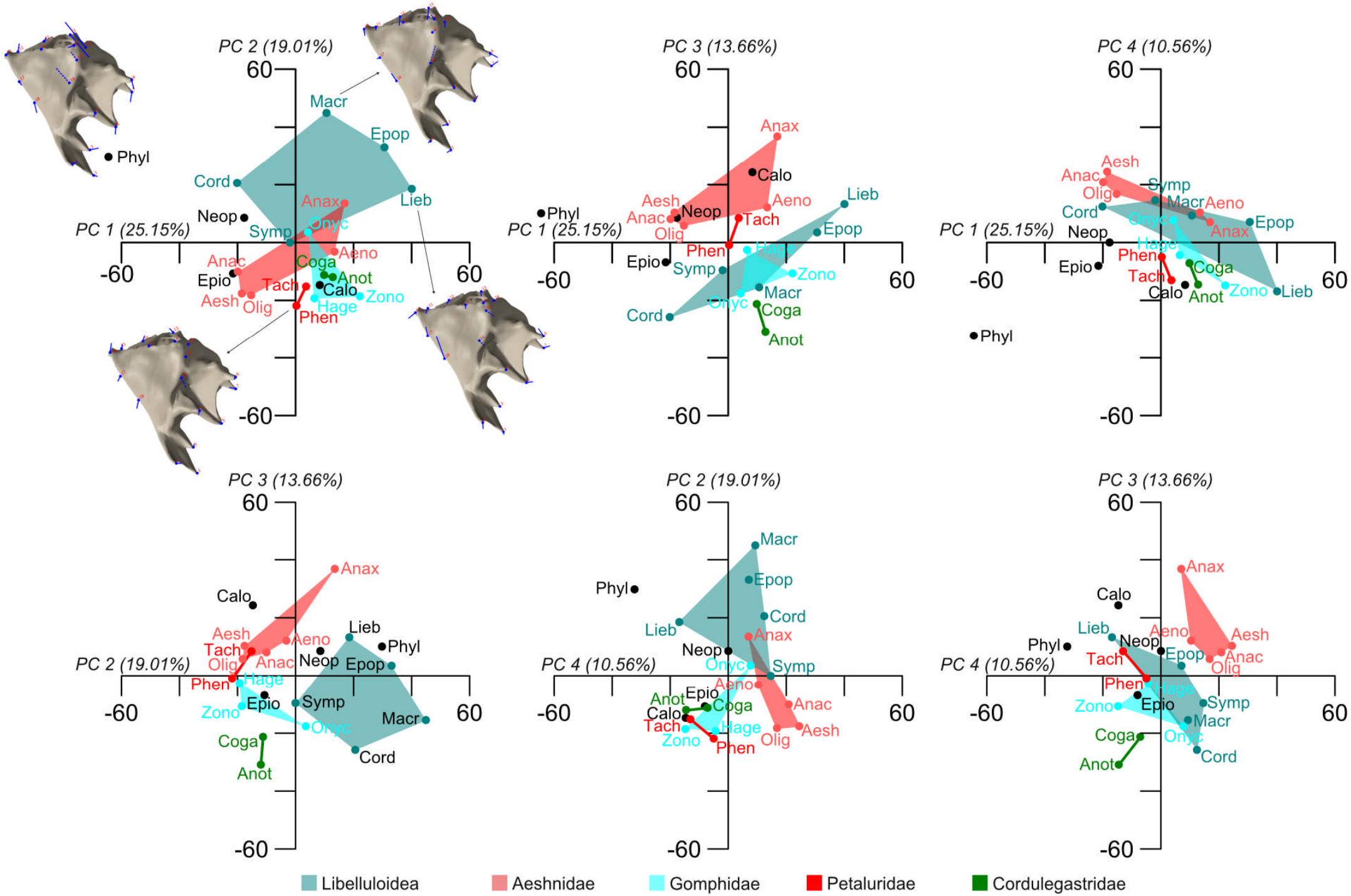
PC 2 (19.01%)
PC 1 (25.15%)
PC 3 (13.66%)
PC 4 (10.56%)
60
-60
Phyl
Macr
Epop
Cord
Lieb
Neop
Anax
Onyc
Symp
Aeno
Anac
Coga
Anot
Epio
Tach
Calo
Zono
Aesh
Olig
Hage
Phen
Libelluloidea
Aeshnidae
Gomphidae
Petaluridae
Cordulegastridae

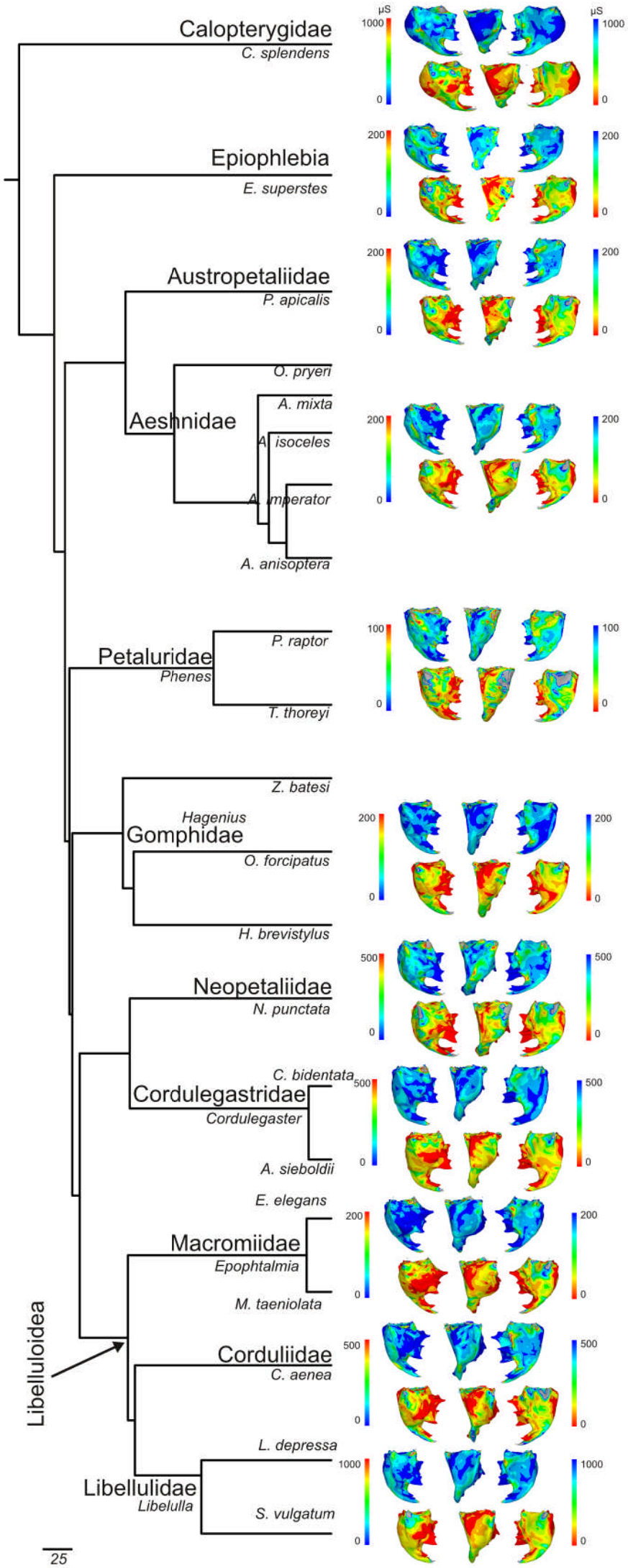
Calopterygidae
C. splendens
Epiophlebia
E. superstes
Austropetaliidae
P. apicalis
O. pryeri
Aeshnidae
A. mixta
A. isoceles
A. imperator
A. anisoptera
Petaluridae
Phenes
P. raptor
T. thoreyi
Z. batesi
Hagenius
Gomphidae
O. forcipatus
H. brevistylus
Neopetaliidae
N. punctata
C. bidentata
Cordulegastridae
Cordulegaster
A. sieboldii
E. elegans
Macromiidae
Epophtalmia
M. taeniolata
Corduliidae
C. aenea
L. depressa
Libellulidae
Libelulla
S. vulgatum
Libelluloidea
μS
1000
0
200
100
500

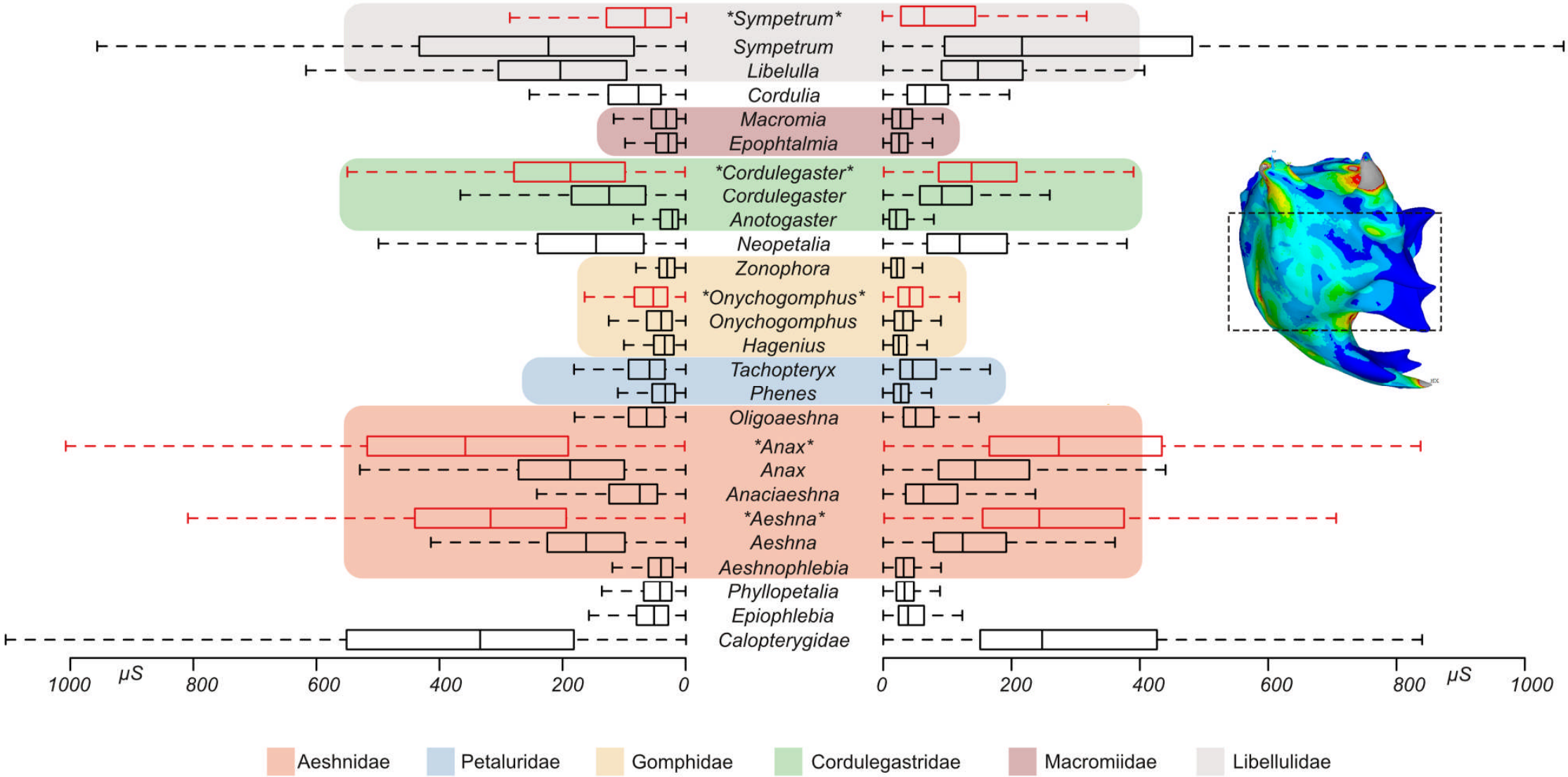
Sympetrum
Sympetrum
Libelulla
Cordulia
Macromia
Epophtalmia
Cordulegaster
Cordulegaster
Anotogaster
Neopetalia
Zonophora
Onychogomphus
Onychogomphus
Hagenius
Tachopteryx
Phenes
Oligoaeshna
Anax
Anax
Anaciaeshna
Aeshna
Aeshna
Aeshnophlebia
Phyllopetalia
Epiophlebia
Calopterygidae
1000 µS 800 600 400 200 0
0 200 400 600 800 µS 1000
Aeshnidae
Petaluridae
Gomphidae
Cordulegastridae
Macromiidae
Libellulidae

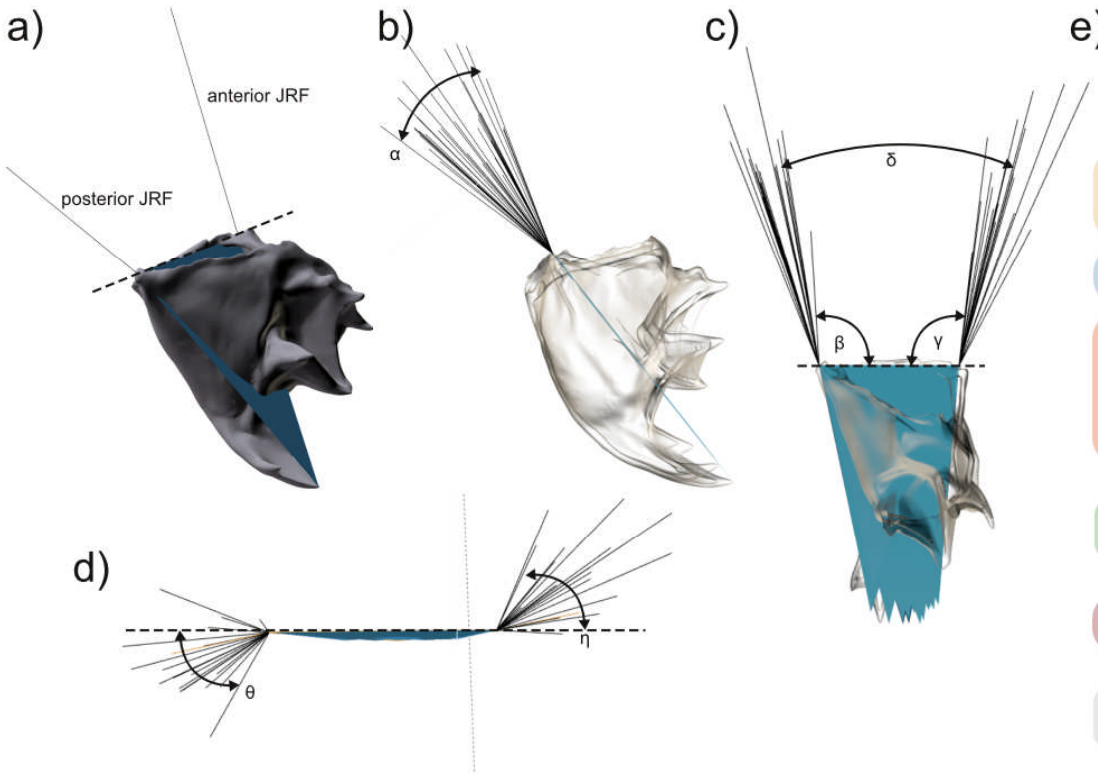

e)

Species	(α)	(β)	(γ)	(δ)	(θ)	(η)	|θ| + |η|	MA
Total range over all species	41.5				90.41	110.96		
Calopteryx virgo	10.7	117.9	102.4	40.3	15.67	13.59	29.27	0.39
Epiophlebia superstes	14.3	104.3	107.9	32.2	34.30	6.66	40.96	0.36
Onychogomphus forcipatus	23.3	98.0	106.7	24.7	21.37	65.40	86.77	0.40
Hagenius brevistylus	7.0	103.1	108.0	31.1	26.26	-9.25	35.50	0.38
Zonophora batesi	7.8	103.0	111.2	34.2	16.56	4.16	20.71	0.39
Phenes raptor	6.6	103.1	106.9	30.0	14.73	7.23	21.96	0.38
Tachopteryx thoreyi	6.9	115.1	102.6	37.6	-15.52	21.70	37.22	0.37
Anax imperator	24.9	97.4	97.9	15.3	39.80	67.67	107.46	0.38
Aeshna mixta	19.8	99.8	106.8	26.6	26.73	49.03	75.76	0.41
Aeshnophlebia anisoptera	19.3	102.5	106.4	28.9	29.65	37.72	67.37	0.38
Anaciaeshna isoceles	15.6	105.6	105.9	31.5	-0.66	45.23	45.90	0.38
Oligoaeschna pryeri	17.4	96.3	106.7	23.1	34.14	40.64	74.77	0.40
Phyllopetalia apicalis	16.3	110.9	108.8	39.7	8.13	32.48	40.61	0.35
Anotogaster sieboldii	22.9	103.1	105.5	28.5	-31.57	-43.31	74.87	0.39
Cordulegaster bidentata	17.8	100.7	101.2	21.9	41.39	34.72	76.11	0.39
Neopetalia punctata	26.3	104.1	104.7	28.7	32.87	49.92	82.79	0.35
Macromia taeniolata	9.2	105.9	99.5	25.4	-9.66	34.04	43.70	0.38
Epophtalmia elegans	7.3	106.5	93.5	20.0	-31.44	29.51	60.95	0.37
Cordulia aenea	19.9	110.2	98.5	28.7	47.59	26.58	74.16	0.37
Sympetrum vulgatum	26.4	119.6	95.4	35.01	-1.39	41.44	42.83	0.41
Libellula depressa	25.4	105.9	99.2	25.1	59.12	31.94	91.05	0.38

Aeshnidae · Petaluridae · Gomphidae · Cordulegastridae · Macromiidae · Libellulidae

Landmark	Definition
1	Distalmost incisivus
2	Subdistal posterior incisivus
3	Subdistal anterior incisivus
4	Molar posteroventral incisivus
5	Molar anteroventral incisivus
6	Molar posterodorsal incisivus
7	Molar anterodorsal incisivus
8	attachment of M. craniomandibularis internus
9	Middle between attachment of M. craniomandibularis internus and posterior mandibular articulation (on the posterior dorsal ridge, PDR)
10	Middle of posterior condyle of posterior mandibular articulation
11	Attachment of M. craniomandibularis externus
12	Middle between posterior mandibular articulation and anterior mandibular articulation
13	Middle of anterior socket of anterior mandibular articulation
14	Middle between anterior mandibular articulation and attachement of M. craniomandibularis internus (on the anterior dorsal ridge, ADR)
15	Middle between anterior mandibular articulation and end of anterior vertical ridge
16	End of anterior vertical ridge
17	Middle between attachement of M. craniomandbularis externus and end of lateral vertical ridge
18	End of lateral vertical ridge

Supplementary online Material
article [TITLE]

Alexander Blanke[1], Helmut Schmitz[2], Alessandra Patera[3], Hugo Dutel[1], Michael J. Fagan[1]

[1] Medical and Biological Engineering Research Group, School of Engineering, University of Hull, Hull HU6 7RX, UK
[2] Institute for Zoology, University of Bonn, Poppelsdorfer Schloss, 53115 Bonn, Germany
[3] Swiss Light Source, Paul Scherrer Institut, Villigen, 5232, Switzerland

Contact: Alexander Blanke; a.blanke@hull.ac.uk

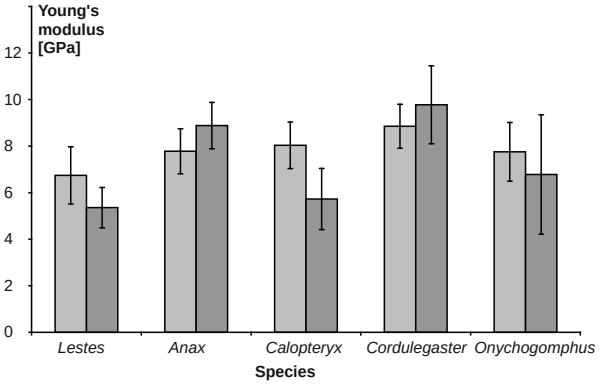

Figure S1 Results for the Young's modulus (GPa) of the nanoindentation experiments for dry (light grey) and rewetted (dark grey) mandibles of five odonate species.

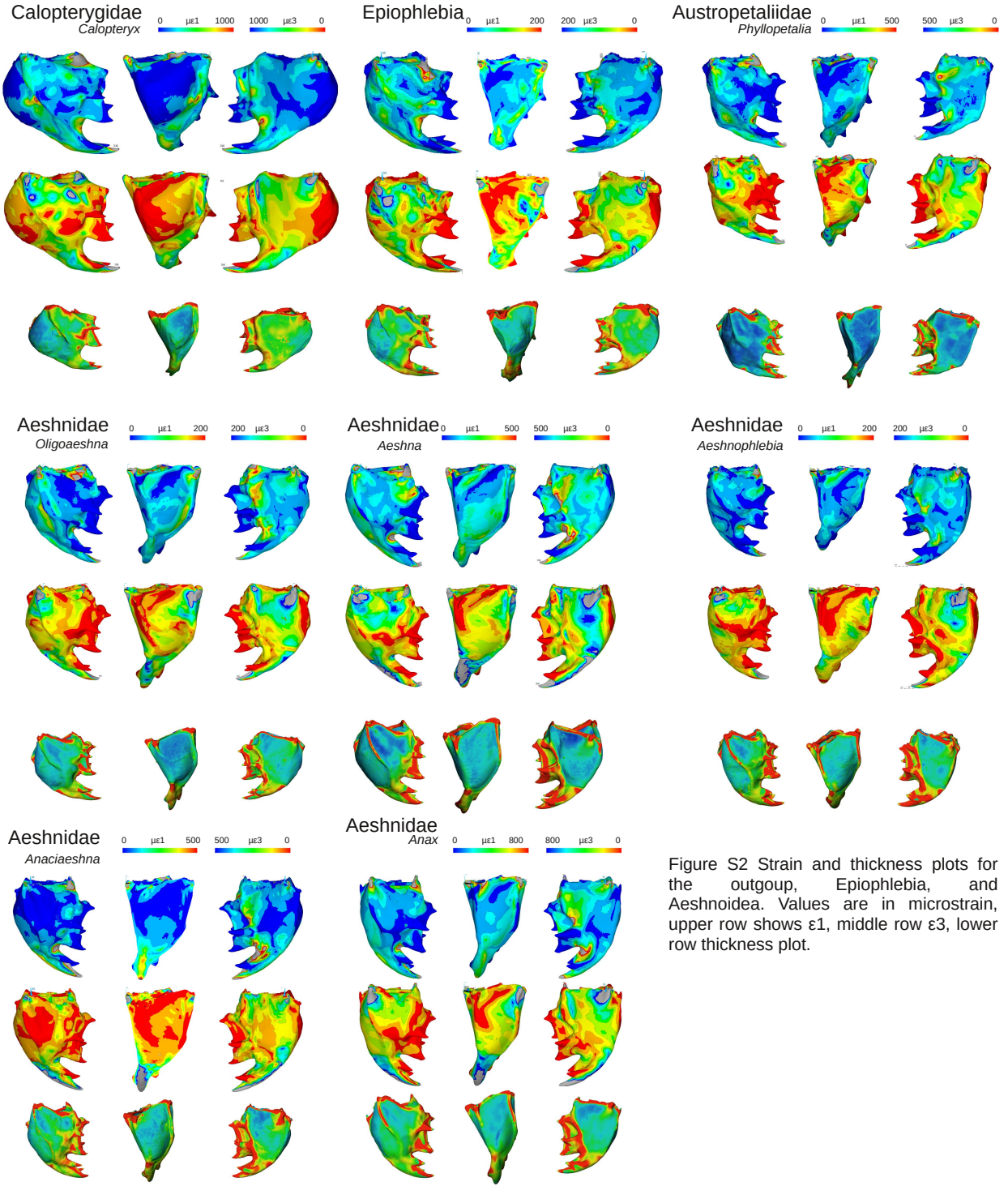

Figure S2 Strain and thickness plots for the outgoup, Epiophlebia, and Aeshnoidea. Values are in microstrain, upper row shows ε1, middle row ε3, lower row thickness plot.

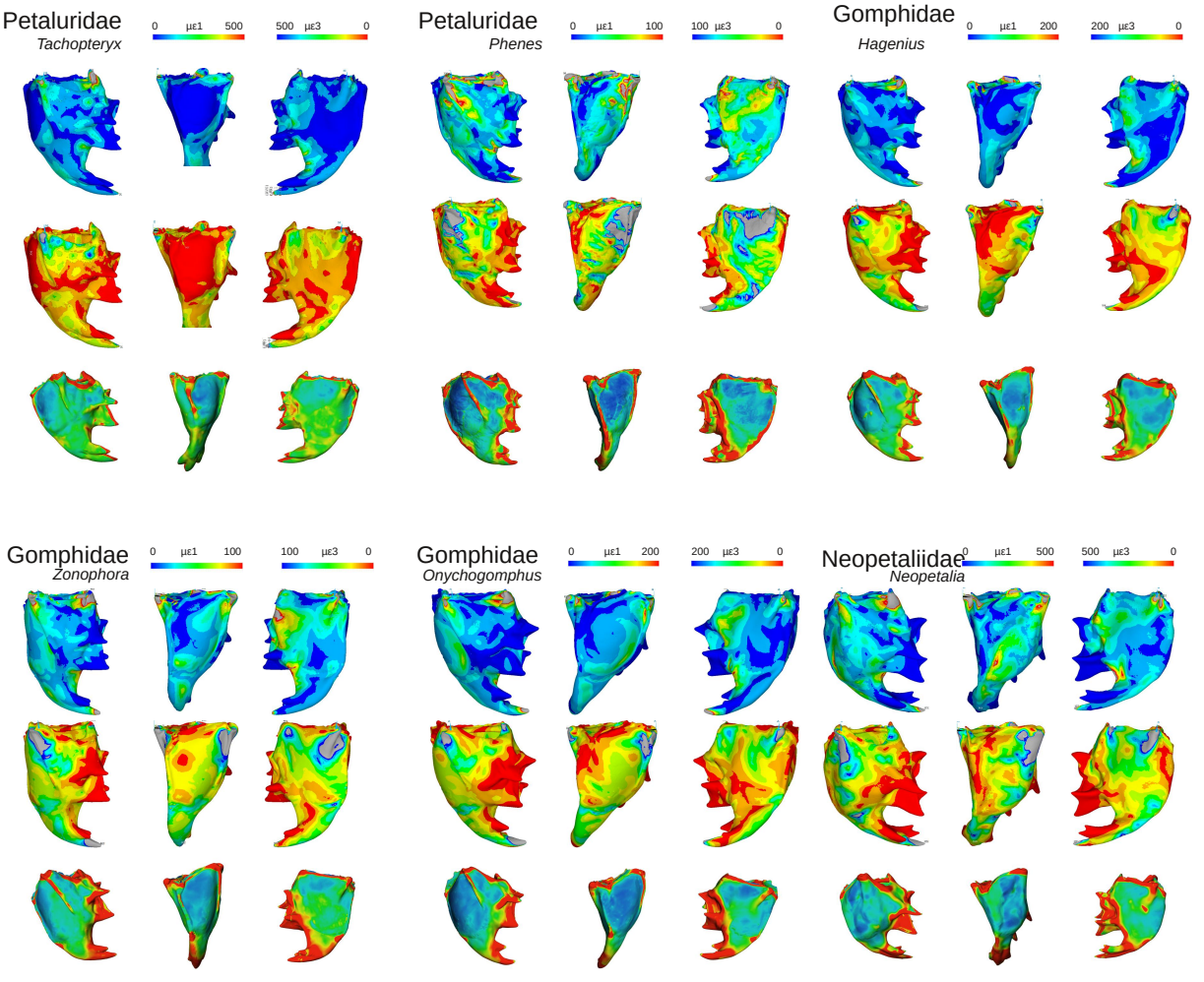

Figure S3 Strain and thickness plots for Petaluridae, Gomphidae and Neopetaliidae. Values are in microstrain, upper row shows ε1, middle row ε3, lower row thickness plot.

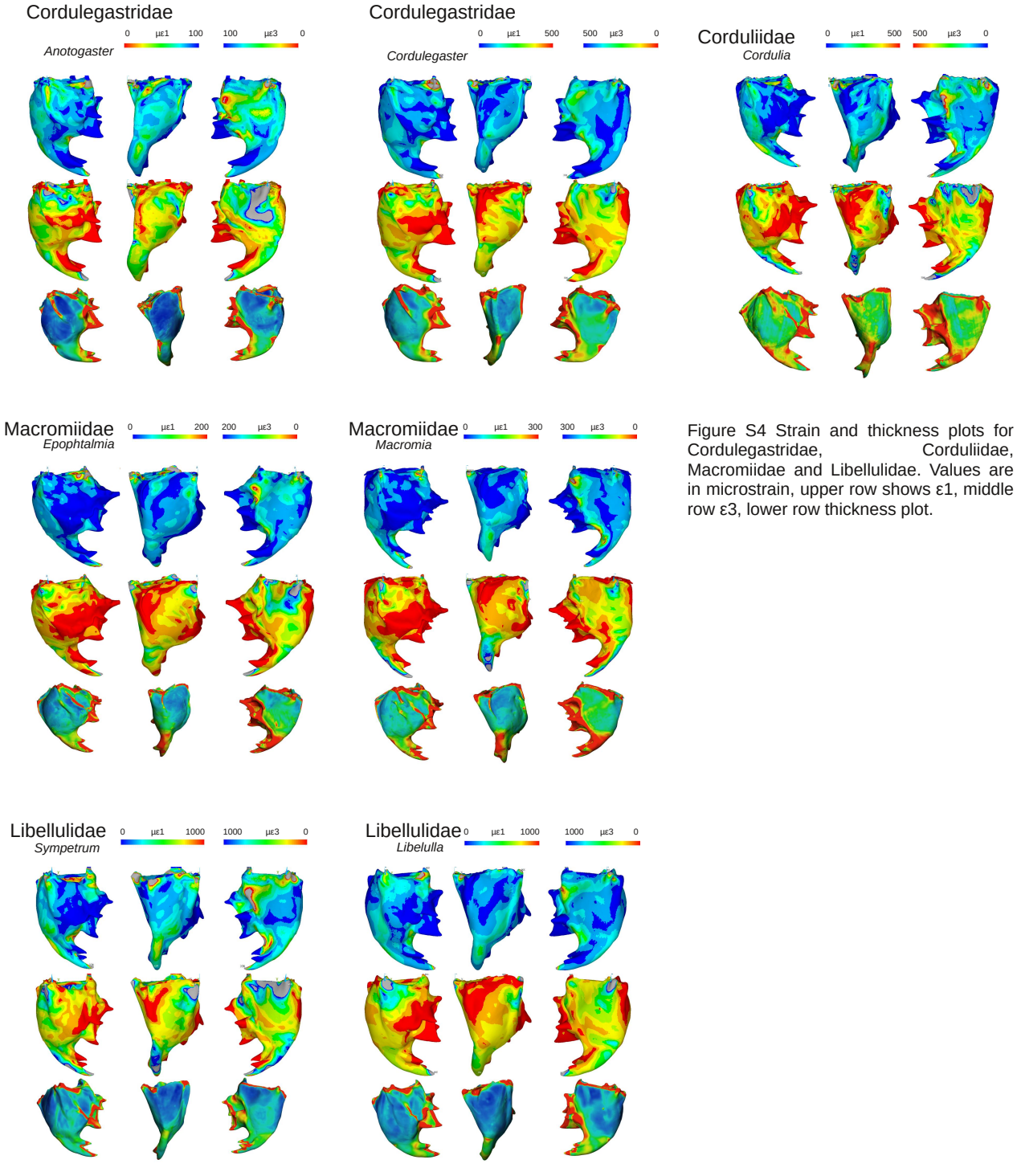

Figure S4 Strain and thickness plots for Cordulegastridae, Corduliidae, Macromiidae and Libellulidae. Values are in microstrain, upper row shows ε1, middle row ε3, lower row thickness plot.

1
2
3
4
5
6
7
8
9
10
12
14
16
18
20
-3000
-2000
-1000
0

1
2
3
4
5
6
7
8
9
10
12
14
16
18
20
0
1000
2000
3000